

Superconductor vortex spectrum from Fermi arc states in Weyl semimetals

Rauf Giwa, Pavan Hosur

Department of Physics, University of Houston, Houston 77204, USA

The vortex core of a type-II superconductor hosts discrete energy levels that carry critical information about the parent normal state. For example, the levels are equally spaced with a zero-point energy equal to half the level spacing if the parent state is an ordinary metal. If the parent state is a massless Dirac fermion instead, the zero-point energy vanishes and an exotic Majorana fermion emerges. Weyl semimetals, three-dimensional topological materials defined by accidental bulk band intersections or Weyl nodes, host a peculiar metal on their surface composed of open Fermi arcs whose end points merge with the bulk Weyl nodes, rather than closed Fermi surfaces. This bizarre structure places Fermi arcs beyond a conventional Hamiltonian description; at the same time, it inspires the fundamental question, “what is the vortex spectrum of a superconductor that descends from a Fermi arc metal?” Here, we answer this question using a powerful semiclassical approach substantiated by lattice numerics. We show that the vortex states form cyclotron-like closed orbits consisting of Fermi arcs on opposite surfaces connected by one-way bulk conduits. The resulting spectrum is governed by the total Berry phase acquired by a wavepacket along this orbit and has characteristic dependences on the Berry phases and penetration depth of the Fermi arcs, bulk Weyl node locations, vortex orientation and sample thickness. Remarkably, eliminating the zero-point energy by manipulating these parameters yields a pair of non-local Majorana fermions, while the thickness dependence disappears at a certain vortex orientation that we dub the “magic angle”. Interestingly, under mild conditions pertinent to many lattice models and materials, non-local Majorana fermions exist precisely at the magic angle.

I. INTRODUCTION

A major milestone in the history of superconductivity was the discovery that it is broadly of two types: type-I superconductors expel magnetic fields completely while type-II superconductors allow magnetic field lines to thread through by developing vortices – topological defects whose winding is unaffected by smooth deformations of the superconducting order parameter. While superficially analogous to vortices in a classical spinning fluid, superconductor vortices are fundamentally quantum mechanical entities with discrete energy levels whose structure encodes properties of the parent superconductor as well as the normal state metal that the superconductor condenses from. In 1964, Caroli-deGennes-Matricon derived the vortex spectrum and proved it to be gapped if the parent metal is an ordinary Fermi gas and superconductivity is conventional [1], which triggered several decades of activity on vortex spectra in other types of metals and superconductors. In contrast, vortices in two dimensional (2D) spinless $p + ip$ superconductors [2] and s -wave superconductors that descend from a 2D Dirac fermion [3] were predicted to host zero energy states that behave like Majorana fermions (MFs). MFs are exotic particles that are their own anti-particles and were first believed to be realized by neutrinos. Their condensed matter realizations, remarkably, form universal building blocks for fault-tolerant quantum computation and make them highly sought-after in solid state systems [4–10]. Recent breakthroughs in Fe-based superconductors have led to a convergence of the above results. These versatile systems not only exhibit strongly

type-II superconductivity with both gapped and gapless vortices, their normal states can also be tuned into various metallic and semimetallic phases in both 2D and 3D [11–24]. Thus, given a metal that can potentially yield type-II superconductivity, a timely and pertinent goal is to determine the vortex spectrum theoretically.

The past decade has seen the rise of a gapless topological state of matter, namely, Weyl semimetals [25–32]. These are 3D systems whose band structure contains accidental crossings between non-degenerate bands at arbitrary points in momentum space. Near such crossings or Weyl nodes, quasiparticles mimic relativistic Weyl fermions but with an effective “speed of light” determined by material’s band parameters. The Weyl nodes carry a chirality or handedness – similar to the chirality of sugar molecules – that influences their response to electromagnetic fields. They are topological objects in the sense that they cannot be destroyed perturbatively as long as translational invariance of the lattice persists, and exhibit various topological responses to electromagnetic fields. General no-go theorems stipulate that generic and inversion symmetric Weyl semimetals contain an even number of Weyl nodes with half of each chirality, whereas in time-reversal (\mathcal{T}) symmetric Weyl semimetals (TWSMs), each Weyl node is accompanied with a time-reversed partner of the same chirality resulting in quadruplets of Weyl nodes.

A striking feature of Weyl semimetals is the presence of surface Fermi arcs (FAs). A FA is a string of zero energy surface states that connects the surface projections of a pair Weyl nodes of opposite chirality. Although it is largely localized on the surface, its penetration depth into the bulk depends strongly on the surface momentum

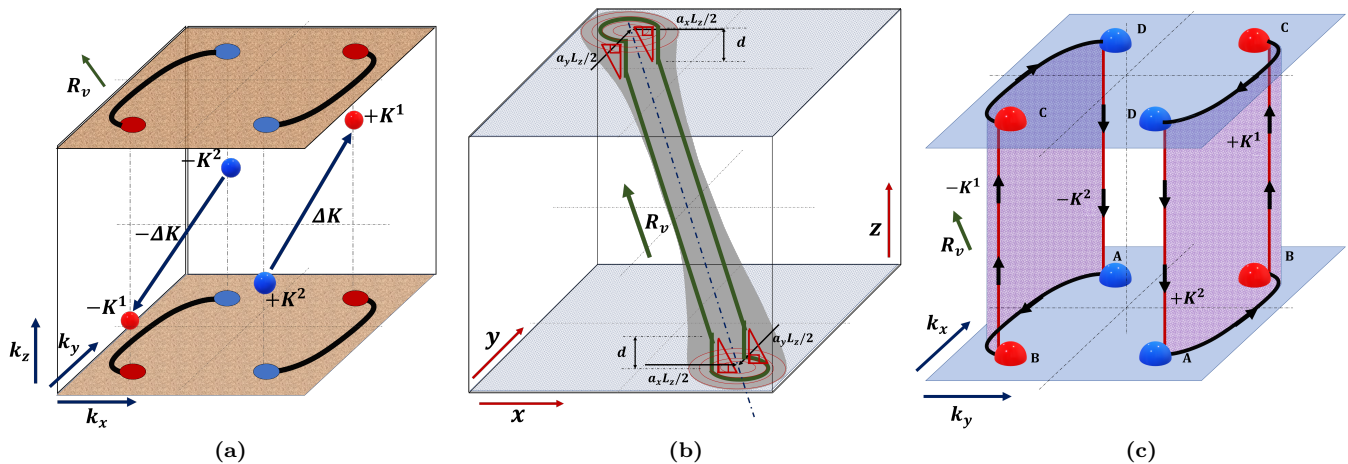


FIG. 1 Schematic of the main results. Left: Illustration of a minimal TWSM with four Weyl nodes in \mathbf{k} -space. Red (blue) spheres at $\pm\mathbf{K}^1$ ($\pm\mathbf{K}^2$) denote right-(left-) handed Weyl nodes, while red (blue) discs denote their projections onto the surface Brillouin zone. Black curves are FAs. Middle: Real space illustration of the vortex (grey tube) and path followed by the wavepacket. The classical path is along the tube axis. Right: Semiclassical orbits in mixed real (z) and momentum (k_x, k_y) space. Each orbit is a closed loop consisting chiral modes in the bulk centered around a pair of Weyl nodes interspersed by surface FAs that connect the projections of these nodes.

and, in fact, diverges at the Weyl node projections. Nonetheless, it resembles an open segment of a 2D Fermi surface, and forms a closed loop with a FA on the opposite surface. As a result, the FAs can be thought of as constituting a 2D metal whose Fermi surface is broken into segments that live on opposite surfaces of a finite slab. At the same time, the bulk penetration of the FA wavefunction causes it to be inextricably coupled with bulk states. The strange Fermiology precludes a strictly surface Hamiltonian; yet, a basic physical question remains: “if the FAs develop fully gapped superconductivity, what is the energy spectrum of a vortex in such a superconductor?”

II. GENERAL VORTEX SPECTRUM

In this work, we answer the above question using a powerful semiclassical approach that eliminates the need for a surface Hamiltonian. We restrict to TWSMs, as \mathcal{T} -symmetry is generically needed for a weak pairing instability in the first place, and propose that the vortex spectrum of a superconductor vortex whose parent metal consists of the FAs is:

$$E_n^\pm = \pm \frac{\Delta_0}{\xi l_{FA}} \left(n + \frac{1}{2} + \frac{\Phi_B + \Phi_S - \Phi_Q}{2\pi} \right) \quad (1)$$

This is our main result. Here, l_{FA} is of order the length of the FA, Δ_0 is the pairing amplitude far from the vortex, ξ is the superconductor coherence length and $n \in \mathbb{Z}$. Additionally, Φ_S is total Berry phase of a “classical” path defined by the FAs on both surfaces that ignores their bulk penetration. The net phase acquired by a wavepacket traversing the bulk is defined as Φ_B . In the simplest case, depicted in Fig. 1, where FAs on opposite surfaces connect the same pairs of Weyl nodes, $\Phi_B = \Delta\mathbf{K} \cdot \mathbf{R}_v$ with $\Delta\mathbf{K}$ connecting the these nodes in momentum space and \mathbf{R}_v connecting the opposite ends of the vortex in real space. Finally, Φ_Q is a quantum correction arising from the penetration of FA states into the bulk, given by

$$\Phi_Q = 2(\Delta\mathbf{K} \times \mathbf{d}) \cdot \frac{\mathbf{R}_v \times \mathbf{d}}{|\mathbf{R}_v \cdot \mathbf{d}|} \quad (2)$$

where $|\mathbf{d}|$ is the average bulk penetration depth of the FA states. Thus, Eq. 1 predicts a generically non-degenerate spectrum with equally spaced energy levels with spacing $\delta = \Delta_0/\xi l_{FA}$, while the zero-point energy is determined by Berry phase of the FAs, Weyl node locations, sample thickness and vortex orientation.

Eq. 1 is inspired by results in Refs. [33], [34] and

[35]. Ref. [34] showed that quasiparticle dynamics

in inhomogeneous superconductors can be faithfully captured by quantizing the semiclassical action for wavepackets traveling in closed orbits in real space. The action, which appears as a phase in the relevant path integral, was shown to consist of three terms: (i) a Bohr-Sommerfeld phase $\oint \mathbf{k}_{\text{classical}} \cdot d\mathbf{r}_{\text{classical}}$ for the classical orbit, (ii) a Berry phase due to rotation of the Nambu spinor, and (iii) a π phase if a unit vortex is encircled. Within a complementary momentum space picture, Ref. [33] proved that, for an arbitrary smooth Fermi surface in the normal state and arbitrary pairing symmetry that ensures a fully gapped state when superconductivity is uniform, the superconductor vortex spectrum is given by $\varepsilon_n^\pm = \pm \frac{\Delta_0}{\xi l_{FS}} \left(n + \frac{1}{2} + \frac{\Phi_{FS}}{2\pi} \right)$ for $l_{FS}\xi \gg 1$, where l_{FS} and Φ_{FS} are the Fermi surface perimeter and Fermi surface Berry phase, respectively. The normal state is assumed to be \mathcal{T} -symmetric, which leads to a pair of Fermi surfaces with opposite Berry phases in the normal state that produce eigenstates related by particle-hole symmetry inside the vortex.

To propose Eq. 1 for a TWSM, we first note that the Bohr-Sommerfeld phase, the π phase from the vortex and the Nambu-Berry phase can be viewed as yielding n , $1/2$ and $\Phi_{FS}/2\pi$, respectively in ε_n . Then, we recall that a Weyl node with chirality $\chi = \pm 1$ produces a chiral MF in the vortex core with chirality χw , where $w = \pm 1$ is the winding number of the vortex [35]. Thus, for $w = 1$, a right-(left-)handed Weyl node produces a chiral MF inside the vortex with upward (downward) group velocity. For a smooth vortex, defined by $\xi^{-1} \ll$ the separation between the Weyl nodes, these chiral modes allow wavepackets to travel between FAs on opposite surfaces without scattering. The smoothness also ensures that a wavepacket on the surface travels along single FA without scattering into other FAs. Thus, the semiclassical orbit naturally involves travel along a FA on the top surface, tunneling through the bulk via a downward chiral MF, FA traversal on the bottom surface followed by tunneling up the bulk via an upward chiral MF. Since a TWSM contains quadruplets of Weyl nodes and even number of FAs on each surface related by \mathcal{T} , such orbits appear in \mathcal{T} -related pairs but with opposite energies in the vortex to ensure that the overall spectrum is particle-hole symmetric. This picture inspires the generalization of Φ_{FS} to $\Phi_B + \Phi_S - \Phi_Q$, the total phase acquired by a wavepacket traversing a closed orbit in mixed real-and-momentum space, as depicted in Fig. 1.

The three components of Φ_{FS} can be understood as follows. The bulk phase Φ_B can be viewed as a phase jump during inter-surface tunneling through the bulk along the chiral Majorana modes. Equivalently, it can be understood as an additional contribution to the Bohr-Sommerfeld phase rather than to Φ_{FS} . Since the chiral modes are tied to the Weyl nodes, Φ_B equals the optical path difference, $\mathbf{K}^1 \cdot \mathbf{R}_v - \mathbf{K}^2 \cdot \mathbf{R}_v = \Delta\mathbf{K} \cdot \mathbf{R}_v$, between semiclassical wavepackets centered at Weyl nodes at \mathbf{K}^1

and \mathbf{K}^2 traversing the bulk portions of the orbit. The natural analog of Φ_{FS} , which captures travel around a 2D Fermi surface, is the Berry phase along the FAs, Φ_{FA} . While Φ_{FA} can be calculated if the exact FA wavefunctions are known, greater insight is obtained by writing $\Phi_{FA} = \Phi_S + 2\Delta\mathbf{K} \cdot \mathbf{d}$, where Φ_S is the Berry phase along the FA acquired by states projected onto the surface and $2\Delta\mathbf{K} \cdot \mathbf{d}$ is the optical path length due to the penetration of FA wavefunctions into the bulk. The penetration also effectively reduces the thickness seen by a wavepacket traveling along the vortex axis by $2d$, as such a wavepacket can tunnel between the vortex core and the surface when it is within distance $\sim d$ from the surface. These two effects of the penetration can be conveniently combined into a quantum correction Φ_Q , given by Eq. (2), which captures the optical path difference between the classical and quantum orbits.

We emphasize several striking aspects of Eq. 1. Firstly, Eq. 1 predicts a gapped spectrum with discrete energy levels for generic parameters even in the thermodynamic limit whereas a pure bulk analysis leads to the prediction of a gapless, continuous spectrum [35]. The latter does yield a discrete spectrum on a finite slab due to quantum confinement. However, the discretization predicted by Eq. 1 is reminiscent of Landau level formation in a 2D electron gas under a magnetic field, rather than conventional finite-size quantization. Secondly, Eq. 1 involves the slab thickness in a highly non-trivial way, namely, within a phase term Φ_B that governs the zero-point energy, while Φ_S and Φ_Q are thickness independent surface terms. The form $\Phi_B = \Delta\mathbf{K} \cdot \mathbf{R}_v$ leads to a remarkable prediction: when the vortex is tilted to a “magic angle” such that $\Delta\mathbf{K} \perp \mathbf{R}_v$, the spectrum becomes independent of the thickness. Under mild conditions, we show shortly that the spectrum at the magic tilt is critical and contains a pair of highly nonlocal MFs.

Besides the FA and chiral mode contribution given by Eq. 1, the vortex spectrum will invariably contain higher energy states in the bulk. In particular, the bulk dispersion due to a single isotropic undoped Weyl node with velocity v is given by $E_{\text{bulk}}^\pm(n_x, n_y, q_z) = \pm \sqrt{\frac{2\hbar v \Delta_0}{\xi} (n_x + n_y) + (\hbar v q_z)^2}$ where $n_x, n_y \in \mathbb{Z} \geq 0$, q_z is measured relative to the Weyl node and the vortex is taken to be along $\hat{\mathbf{z}}$ [35]. The case $n_x = n_y = 0$ corresponds to the chiral MF mentioned earlier and is the only gapless mode, while nonchiral modes lie above the bulk gap $E_g = \sqrt{2\hbar v \Delta_0}/\xi$. Clearly, $E_g \gg \delta$ if $l_{FA} \gg \sqrt{\Delta_0/\hbar v \xi} \sim \xi^{-1}$, assuming standard Ginzburg-Landau theory. In other words, the smooth vortex limit of $l_{FA}\xi \gg 1$, where Eq. 1 is expected to hold, also ensures that non-chiral bulk modes are at parametrically higher energies. Thus, Eq. 1 is expected to be the vortex spectrum for a smooth vortex at low energies.

We now substantiate our claim via exact

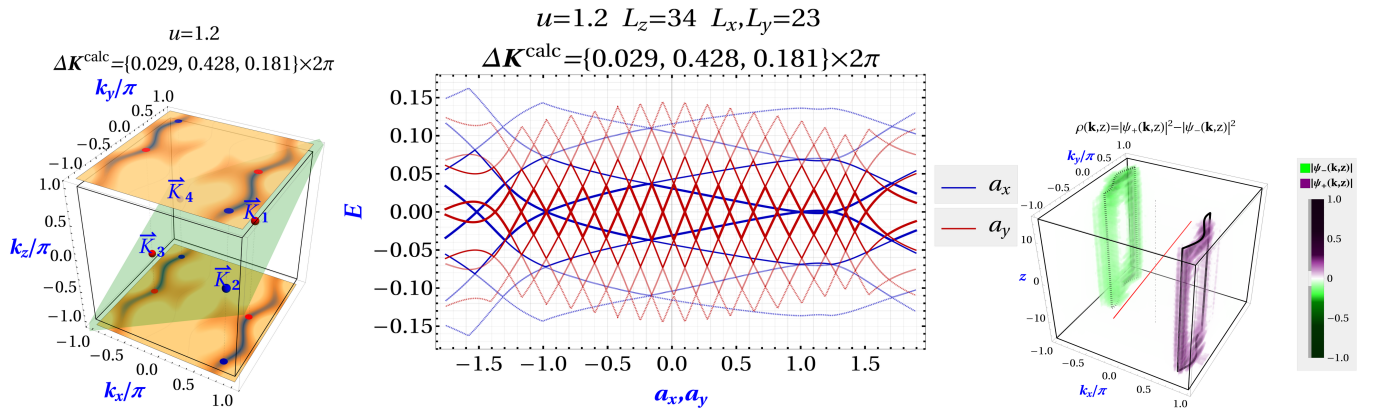


FIG. 2 Numerical verification of the main results. Left: Normal state band structure showing four bulk Weyl nodes (red and blue spheres), all at different k_z , and surface FAs connecting them. The four nodes lie on the green plane, which is clearly not parallel to the surface. Middle: Vortex spectrum of a $L_x \times L_y \times L_z = 23 \times 23 \times 34$ system as the vortex is tilted separately towards the x -axis and the y -axis, where $\tan^{-1} a_i$ ($i = x, y$) is the tilt angle towards the i -axis. Right: Net probability density of the two lowest energy wavefunctions in (k_x, k_y, z) space at $a_y = 1.25$, marked ‘X’ in the middle figure, obtained by Fourier transforming the 3D real space wavefunctions with respect to x and y .

diagonalization calculations on the lattice model described in detail in Methods. Fig. 2(left) shows the FAs and Weyl nodes in a minimal TWSM with four Weyl nodes located at $\pm \mathbf{K}^1$ and $\pm \mathbf{K}^2$. We have chosen parameters such that all nodes are at different k_z , where $\hat{\mathbf{z}}$ is the surface normal, and $|\Delta K_x| \ll |\Delta K_y|$ where $\Delta \mathbf{K} = \mathbf{K}^1 - \mathbf{K}^2$. Calculating the vortex spectrum is computationally costly; this limits us to relatively small systems and short ξ which, in turn, causes level spacings to be unequal for modest values of n in Eq. 1. We circumvent this limitation by studying the spectrum as a function of vortex orientation and fitting the tilt angles where zero modes occur to their expected locations according to Eq. 1. As we describe below, the expectations and observations show remarkable agreement.

Fig. 2(middle) shows the vortex spectrum for a finite slab when a vortex, initially along $\hat{\mathbf{z}}$, is tilted separately

towards the x - and the y -axis. The tilt is parametrized as $\mathbf{R}_v = (a_x, a_y, 1)L_z$. Tilting towards the positive y -axis ($a_x = 0, a_y > 0$) produces numerous level crossings, which is consistent with $\Phi_B = (\Delta K_y a_y + \Delta K_z)L_z$ changing by many multiples of 2π as a_y varies. In contrast, the spectrum varies weakly when the vortex is tilted towards the x -axis, which is consistent with $\Phi_B = \Delta K_x a_x L_z$ varying negligibly with a_x since ΔK_x itself is small. In Fig. 2(c), we plot the wavefunctions of a pair of levels with equal and opposite energies in (k_x, k_y, z) space. The levels, which are related by particle-hole symmetry of the superconductor, are clearly localized around semiclassical orbits related by time-reversal. This confirms the picture that motivated Eq. 1, namely, that the vortex spectrum follows from quantizing semiclassical orbits in mixed real-and-momentum space, and that semiclassical orbits related by time-reversal turn into pairs of particle-hole conjugate quantum eigenstates.

To resolve the Berry phase dependence of the zero point energy, we note that Eq. 1 predicts a pair of zero modes, as seen for the y -leaning vortex, whenever $\Phi_{\text{tot}} = \Phi_B + \Phi_S - \Phi_Q$ equals an odd multiple of π . In this geometry, $\Phi_B = (\Delta K_y a_y + \Delta K_z)L_z$, Φ_S is determined by the band structure and is a_y - and L_z -independent, and $\Phi_Q \propto a_y$ and L_z -independent. An immediate prediction that follows is that Φ_{tot} becomes independent of L_z at the “magic angle”, $\theta = -\tan^{-1}(\Delta K_z/\Delta K_y)$. Interestingly, we see in Fig. 3(top) that zero modes exist precisely at the magic tilt, $a_y \approx 0.424$, implying that $\Phi_S - \Phi_Q = \pi \pmod{2\pi}$ at this tilt. We proceed to fit

Φ_{tot} to a suitable function of a_y and L_z and extract the values of ΔK_y , ΔK_z and Φ_S . These values show good agreement with the values determined directly from the normal state band structure, as indicated in Fig. 3(bottom). Further details of the fitting procedure are in Methods.

It is instructive to compare the above result with the ones for quantum oscillations due to FAs in Weyl semimetals [36–38]. There, a magnetic field B induces cyclotron orbits involving surface FAs and bulk chiral modes. The oscillation period in $1/B$ equals the area enclosed by FAs on opposite surfaces while the slab

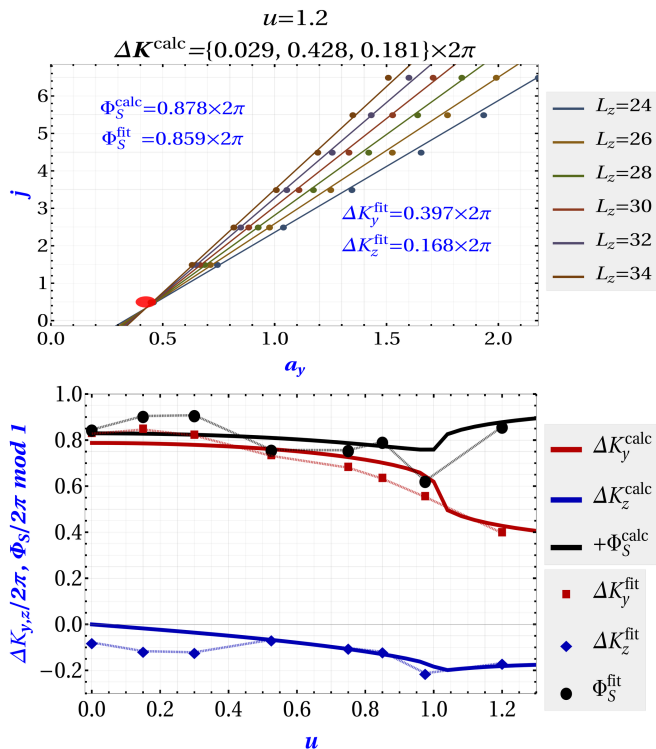


FIG. 3 Numerical fits. Top: Zero modes indices (n) vs a_y fit well to straight lines for each L_z . The lines intersect at $a_y = 0.424$, which defines the magic tilt. The symmetries of the model guarantee zero modes precisely at this tilt. Fitting the slopes and intercepts, again, to straight lines in L_z allows extracting Φ_S , ΔK_y and ΔK_z numerically, which match well with their values calculated from the band structure. Bottom: The matches are good for a wide range of band parameters, parameterized by u . See Methods for further details of the band structure calculations and fitting procedure.

thickness modifies the oscillation phase via a Bloch phase acquired during the bulk transport. In a purely quantum picture, the magnetic field produces discrete Landau levels whose spacing is affected by the area enclosed by the FAs and the zero point energy captures the bulk Bloch phase. Similarly, for a superconductor vortex, the bulk portion of the orbit induces a Bloch phase that modifies the zero point energy of the vortex spectrum. However, the level spacing is expected to be governed by the FA length rather than the area enclosed. Moreover, particle-hole symmetry of the superconductor forbids oscillations in the density of states as Δ_0 or ξ are varied. Instead, oscillations occur as the Berry phases Φ_B , Φ_S and Φ_Q change. The first and the third can be varied by tilting while the second is fixed for a given material.

III. NONLOCAL MAJORANA FERMIONS

MFs are exotic particles that are their own anti-particles and were first proposed – but are yet to be found – in the context of neutrino physics. In recent years, the interplay of band topology, spin-orbit coupling and superconductivity has paved a new route to these elusive particles. Following realizations in semiconductor nanowire-superconductor heterostructures [39–41], MFs were recently seen for the first time in a three-dimensional (3D) system – at the ends of vortices in the bulk superconductor $\text{FeSe}_{0.45}\text{Te}_{0.55}$ [11, 12, 15, 19]. In addition, they have been predicted to occur inside superconductor vortex cores on the surfaces of topological insulators [3], metals with strong spin-orbit coupling [33, 42], and recently, TWSMs proximate to a topological insulators [35]. Besides their fundamental importance, MFs have been shown to form universal building blocks for fault-tolerant quantum computation, which inspires a continuing search for systems which host them. While the route to MFs in all the above examples has been as topologically protected localized zero energy bound states trapped in topological defects such as superconductor vortices and domain walls [5–7, 10, 16, 33, 40, 41, 43–54], we now show that the semiclassical orbits described in this work give rise to a novel class of MFs that are nonlocal in mixed real and momentum space.

As depicted in Fig. 1(right) and computed numerically in Fig. 2(right), semiclassical orbits in a TWSM appear in pairs related by time-reversal. Heuristically, since energy is conjugate to time, the two orbits in a pair yield quantum eigenstates $|n+\rangle$ and $|n-\rangle$ with opposite energies E_n^+ and E_n^- that guarantee a particle-hole symmetric spectrum as required for a superconductor. More precisely, they satisfy

$$\mathcal{C}|n, \lambda\rangle = |n, -\lambda\rangle, H_v|n, \lambda\rangle = E_n^\lambda|n, \lambda\rangle; \lambda = \pm \quad (3)$$

where \mathcal{C} denotes charge conjugation, H_v is the vortex Bogoliubov-deGennes Hamiltonian and E_n^λ is given by Eq. 1. This behavior is a mixed real-and-momentum space generalization of the correspondence between particle-hole conjugate states in the vortex spectrum and Kramer’s conjugate Fermi surfaces in the normal state [33].

A striking behavior arises whenever $E_n^\lambda = 0$. At these points, “cat” superpositions of the eigenstates are simultaneous eigenstates of H_v and \mathcal{C} since

$$\mathcal{C}\left(\frac{|n, +\rangle \pm |n, -\rangle}{\sqrt{2}}\right) = \pm \left(\frac{|n, +\rangle \pm |n, -\rangle}{\sqrt{2}}\right) \quad (4)$$

As a result, $|\chi_{n,\pm}\rangle = \frac{1}{\sqrt{2}}(|n, +\rangle \pm |n, -\rangle)$ are MFs. These MFs have a peculiar non-local structure as they are composed of $|n, \pm\rangle$, which themselves have a non-local structure in mixed real-and-momentum space. They are

not protected by symmetry; rather, they appear at a series of critical points as a function of the vortex tilt. We can view them as analogs of the critical MF wires that occur at topological phase transitions between trivial and topological vortices which, respectively, lack and host surface MFs. This interpretation, however, raises another question: what topological phases do $|\chi_{n,\pm}\rangle$ separate?

For general band and vortex parameters, the vortex belongs to class D in the Altland-Zirnbauer classification as $\mathcal{C}^2 = +1$ while \mathcal{T} is broken by the vortex. Since the finite thickness is crucial to the physics described here, the vortex is effectively a zero dimensional superconductor and must be viewed as a large superconducting quantum dot. This is in contrast to previous studies of superconductor vortices in metals [21, 33], semimetals [35, 55–57] and insulator surfaces [3, 58], where they are viewed as 1D superconductors in class D. Class D superconductors in zero dimensions are characterized by a \mathbb{Z}_2 topological invariant, $\nu = 0, 1$, where the trivial and topological phases correspond to even and odd fermion parity [59]. Thus, the “phases” separated by the MFs $|\chi_{n,\pm}\rangle$ carry even and odd numbers of fermions.

IV. MAJORANA FERMIONS AT THE MAGIC ANGLE

In real materials, the detailed shape and connectivity of FAs depends on the local boundary conditions. Nonetheless, significant insight can be obtained by considering a slab of a material exposed to vacuum on either side. This approach is routinely adopted in theoretical treatments of topological phases and is pertinent when the topological material either couples weakly to the substrates or is sandwiched between identical substrates. In Weyl semimetals, a common feature that appears in this limit is exact overlap between FAs on the top and the bottom surfaces.

We first describe the conditions that protect the coincidence of FAs on opposite surfaces, assumed normal to \hat{z} , in generic TWSMs. Suppose the coinciding FAs are related by an operation \mathcal{P} :

$$\mathcal{P}|t(\mathbf{k})\rangle = e^{i\eta(\mathbf{k})}|b(\mathbf{k})\rangle; \mathcal{P}|b(\mathbf{k})\rangle = e^{i\eta'(\mathbf{k})}|t(\mathbf{k})\rangle \quad (5)$$

where $|t(\mathbf{k})\rangle, |b(\mathbf{k})\rangle$ denote the exact FA states on the top and bottom surfaces respectively including their spatial profile in z , $\mathbf{k} = (k_x, k_y)$ is the in-plane momentum and $\eta(\mathbf{k}), \eta'(\mathbf{k})$ are phases. \mathcal{P} must change $z \rightarrow -z$ to interchange the FAs, must preserve \mathbf{k} so that it can protect overlap between FAs of arbitrary shape, and must not change k_z to preserve the locations of the bulk Weyl nodes. This restricts \mathcal{P} to be anti-unitary and of the form $\mathcal{P} = \mathcal{T}\tilde{I}$, where \tilde{I} denotes spatial inversion followed by a local unitary transformation within a unit

cell. Next, suppose $[\mathcal{P}, \hat{H}(\mathbf{k})] = 0$, where $\hat{H}(\mathbf{k})$ is the Bloch Hamiltonian matrix at \mathbf{k} . \mathcal{P} would then conserve energy and cause the FAs it relates to disperse in the same direction. However, this leads to a contradiction as each point on the FA contour constitutes an edge state of a 2D Chern defined on a momentum-space sheet that encloses a Weyl node and edge states of Chern insulators must necessarily disperse in opposite directions. If $\{\mathcal{P}, \hat{H}(\mathbf{k})\} = 0$ instead, \mathcal{P} can protect the coincidence of FAs at zero energy and allow them to disperse in opposite directions. Thus, protected overlap between FAs on opposite surfaces in generic TWSMs requires a particle-hole symmetry – an anti-unitary operation that anti-commutes with the tight-binding Hamiltonian – at each \mathbf{k} . We now show that if $\mathcal{P}^2 = -1$, so that $\eta'(\mathbf{k}) - \eta(\mathbf{k}) = \pi$ and $\hat{H} \in \text{CII}$ in the Altland-Zirnbauer classification, a striking phenomenon occurs: zero modes exist in the vortex spectrum precisely at the magic angle, as seen in Fig. 3(left) at $a_y \approx 0.424$.

At the magic angle, Eq. (2) implies $-\Phi_Q = 2\Delta\mathbf{K} \cdot \mathbf{d}$, the optical path due to penetration of the FA states into the bulk. As a result, $\Phi_S - \Phi_Q = \Phi_{FA}$, the total Berry phase from the FA states. We now calculate Φ_{FA} directly instead of splitting it as $\Phi_{FA} = \Phi_S + 2\Delta\mathbf{K} \cdot \mathbf{d}$ and show that $\Phi_{FA} = \pi$ if $\mathcal{P}^2 = -1$. Explicitly,

$$\begin{aligned} \Phi_{FA} &= \int_{\mathbf{K}_\perp^1}^{\mathbf{K}_\perp^2} i \left(\langle t(\mathbf{k}) | \partial_{k_{FA}} t(\mathbf{k}) \rangle - \langle b(\mathbf{k}) | \partial_{k_{FA}} b(\mathbf{k}) \rangle \right) dk_{FA} \\ &= \eta(\mathbf{K}_\perp^2) - \eta(\mathbf{K}_\perp^1) \end{aligned} \quad (6)$$

using Eq. (5), where k_{FA} is the momentum along the FA, $\mathbf{K}_\perp^i \equiv (K_x^i, K_y^i)$. A Berry phase generically is gauge-invariant only for closed paths whereas the FAs are open contours. Thus, $\Phi_{\text{top}} = \int_{\mathbf{K}_\perp^1}^{\mathbf{K}_\perp^2} i \langle t(\mathbf{k}) | \partial_{k_{FA}} t(\mathbf{k}) \rangle dk_{FA}$ and $\Phi_{\text{bottom}} = \int_{\mathbf{K}_\perp^2}^{\mathbf{K}_\perp^1} i \langle b(\mathbf{k}) | \partial_{k_{FA}} b(\mathbf{k}) \rangle dk_{FA}$ are not gauge-invariant, which makes Φ_{FA} naively ambiguous. To resolve this paradox, we note that each point on each FA can be understood as an edge state of a Chern insulator. While a single edge of a Chern insulator violates gauge invariance and exhibits a 1D chiral anomaly, opposite edges together respect gauge invariance.

To determine $\eta(\mathbf{K}_\perp^2) - \eta(\mathbf{K}_\perp^1)$, we consider the action of \mathcal{P} on the bulk states. Since Weyl nodes at \mathbf{K}^1 and \mathbf{K}^2 have opposite chiralities, an electron Fermi surface around \mathbf{K}^1 , carries the same Chern number as a hole Fermi surface that encloses \mathbf{K}^2 . As a result, a smooth set of unitary transformations exists that deform Bloch states on the former into Bloch states on the latter. Shrinking these Fermi surfaces to vanishing volume around the Weyl nodes then reduces the unitary transformations to a pure phase, $e^{i\alpha}$, which implies that an upward dispersing chiral mode at \mathbf{K}^1 has the same Bloch ket as a downward dispersing chiral mode at \mathbf{K}^2 , and vice versa. Now, the FA states smoothly merge with

the bulk states at the Weyl nodes, so the upward chiral modes at both \mathbf{K}^1 and \mathbf{K}^2 are simply the end-points of the bottom FA, $|b(\mathbf{K}^1)\rangle$ and $|b(\mathbf{K}^2)\rangle$, respectively, while the downward modes are $|t(\mathbf{K}^1)\rangle$ and $|t(\mathbf{K}^2)\rangle$, or vice-versa. Therefore, $|t(\mathbf{K}^1)\rangle = e^{i\alpha}|b(\mathbf{K}^2)\rangle$ and $|t(\mathbf{K}^2)\rangle = e^{i\alpha}|b(\mathbf{K}^1)\rangle$, which yields

$$\begin{aligned} e^{i\eta(\mathbf{K}_\perp^2)} &= \langle b(\mathbf{K}_\perp^2) | \mathcal{P} | t(\mathbf{K}_\perp^2) \rangle \\ &= \langle t(\mathbf{K}_\perp^1) | \mathcal{P} | b(\mathbf{K}_\perp^1) \rangle \\ &= -e^{i\eta(\mathbf{K}_\perp^1)} \end{aligned} \quad (7)$$

or $\Phi_{FA} = \eta(\mathbf{K}_\perp^2) - \eta(\mathbf{K}_\perp^1) = \pi$, where we have used Eq. (5) with $\eta'(\mathbf{k}) = \eta(\mathbf{k}) + \pi$, which follows from $\mathcal{P}^2 = -1$.

V. METHODS

A. Numerical calculation of vortex spectrum

We support our general claims of Eq. 1 with numerics on an orthorhombic lattice model of a tilted superconducting vortex on a TWSM defined by 8. The lattice model contains two layers per unit cell in the z -direction, assumed to be the surface normal, and is described by the bulk Bloch Hamiltonian and spectrum

$$\begin{aligned} H_0(\mathbf{k}, k_z) &= \boldsymbol{\tau} \cdot \mathbf{d}(\mathbf{k}, k_z) - \mu \\ \varepsilon_\pm^2(\mathbf{k}, k_z) &= \left(\sqrt{v_x^2 \sin^2 k_x + v_y^2 \sin^2 k_y \pm \ell} \right)^2 + d_\perp^2(\mathbf{k}, k_z) \end{aligned} \quad (8)$$

where $\mathbf{k} = (k_x, k_y)$, $\tau_z = \pm 1$ for the two layers of the bilayer, $d_x(\mathbf{k}, k_z) = m_0 + \beta_x \cos k_x + \beta_y \cos k_y + \beta_z \cos k_z$, $d_y(\mathbf{k}, k_z) = u_x \sin k_x + u_y \sin k_y - u_z \sin k_z$, $d_\perp^2(\mathbf{k}, k_z) = |d_x(\mathbf{k}, k_z)|^2 + |d_y(\mathbf{k}, k_z)|^2$ and $d_z(\mathbf{k}, k_z) \equiv d_z(\mathbf{k}) = \sigma_x v_x \sin k_x + \sigma_y v_y \sin k_y - \ell$ denotes purely in-plane hopping that captures spin-orbit coupling through spin Pauli matrices $\sigma_{x,y}$ and inversion symmetry breaking through the term $\propto \ell$. $H_0(\mathbf{k}, k_z)$ can be understood as two copies – one for each spin – of the bilayer prescription for Weyl semimetals described in Ref. [60]. It preserves time-reversal symmetry ($\mathcal{T} = \sigma_y \mathbb{K}$) but breaks all spatial symmetries for general (u_x, u_y, u_z) . It preserves a chiral symmetry, $\tilde{I} = \tau_y \sigma_z \otimes (\mathbf{r} \rightarrow -\mathbf{r})$, which is better understood as spatial inversion about a point between the layers of the bilayer, $\tau_x \sigma_z \otimes (\mathbf{r} \rightarrow -\mathbf{r})$, followed by a gauge transformation $\psi \rightarrow e^{i\tau_z \sigma_z \frac{\pi}{2}} \psi$. The resulting particle-hole symmetry, $\mathcal{P} = \mathcal{T} \tilde{I}$, causes FAs on opposite surfaces to coincide.

The prescription dictates that the bulk Weyl nodes occur when $\varepsilon_{-\text{sgn}(\ell)}(\mathbf{k}) = 0$, while surface FAs occur between projections of the Weyl nodes along curves where $d_z(\mathbf{k})$ has zero eigenvalues. For $u_x = u_y = 0$, all the nodes lie at either $k_z = 0$ or π , while non-zero u_x, u_y place the Weyl nodes into

separate k_z planes. In our calculations, we choose band parameters $\{v_x, v_y, \ell\} = \{3.53, 2.48, 3.00\}$, $\{m_0, \beta_x, \beta_y, \beta_z\} = \{1.000, -0.939, 0.371, 0.652\}$, $\{u_x, u_y, u_z\} = \{u \cos 0.20\pi, u \sin 0.20\pi, 1.00\}$, and tune u to generate different Weyl node and FA configurations.

To determine the vortex spectrum, we diagonalize the Bogoliubov-deGennes Hamiltonian

$$H = \pi_z H_0(\mathbf{k}, k_z) + H_V(\mathbf{r} - \mathbf{a}z) \quad (10)$$

in real space, where π_i are Pauli matrices in Nambu space and

$$\begin{aligned} H_v(\mathbf{r} - \mathbf{a}z) &= \Delta(|\mathbf{r} - \mathbf{a}z|) \times \\ &\quad \begin{pmatrix} \pi_x \cos \Theta(\mathbf{r} - \mathbf{a}z) \\ +\pi_y \sin \Theta(\mathbf{r} - \mathbf{a}z) \end{pmatrix} \end{aligned} \quad (11)$$

captures the vortex. Here, $\Delta(\mathbf{r} - \mathbf{a}z) = \Delta_0 \tanh(|\mathbf{r} - \mathbf{a}z|/\xi)$ and the vortex orientation is parametrized as $\mathbf{R}_v = L_Z(a_x, a_y, 1)$.

B. Fitting zero modes to Eq. 1

Direct numerical verification of Eq. 1 involves diagonalizing H_v in real space and comparing the resulting energy spectrum with Eq. 1. However, the lack of translation invariance in all directions limits us to relatively small ξ , which causes departure from the semiclassical limit and hence, from Eq. 1 at modest energies. We bypass this limitation by varying the vortex orientation and comparing the locations of the zero modes with the predictions of Eq. 1. This way, we always probe only the lowest few energy levels, which are less sensitive to departure from the semiclassical limit.

For fixed band parameters in the normal state, we set $a_x = 0$ and vary a_y between $\pm L_y/L_z$; for larger a_y , the vortex enters and exits from the side surfaces. Zero modes exist at regular intervals of a_y , which we expect to correspond to $\Phi_B + \Phi_S - \Phi_Q$ sweeping past an odd multiple of π . We repeat an analogous procedure for a_x with $a_y = 0$, but find no zero modes, which is consistent with the prediction of Eq. 1 for $\Delta K_x \approx 0$ in the band structure.

The results for $a_y \neq 0$, $a_x = 0$ are shown in Fig. 4. Defining $j = \Phi_{\text{tot}}/2\pi$, we assign consecutive half-integer j values to the zero modes for fixed L_z . For each L_z , $\Phi_{\text{tot}}(L_z)$ fits excellently to separate straight lines for $a_y > 0$ (right tilt) and $a_y < 0$ (left tilt):

$$\Phi_{\text{fit}}(L_z, a_y) = m(L_z) a_y + c(L_z) \quad (12)$$

The slope and intercept, $m(L_z)$ and $c(L_z)$, are each found to be almost perfect straight line functions of L_z . The upshot is that Φ_{fit} is of the form

$$\Phi_{\text{fit}}(L_z, a_y) = A + B a_y + C L_z + D a_y L_z \quad (13)$$

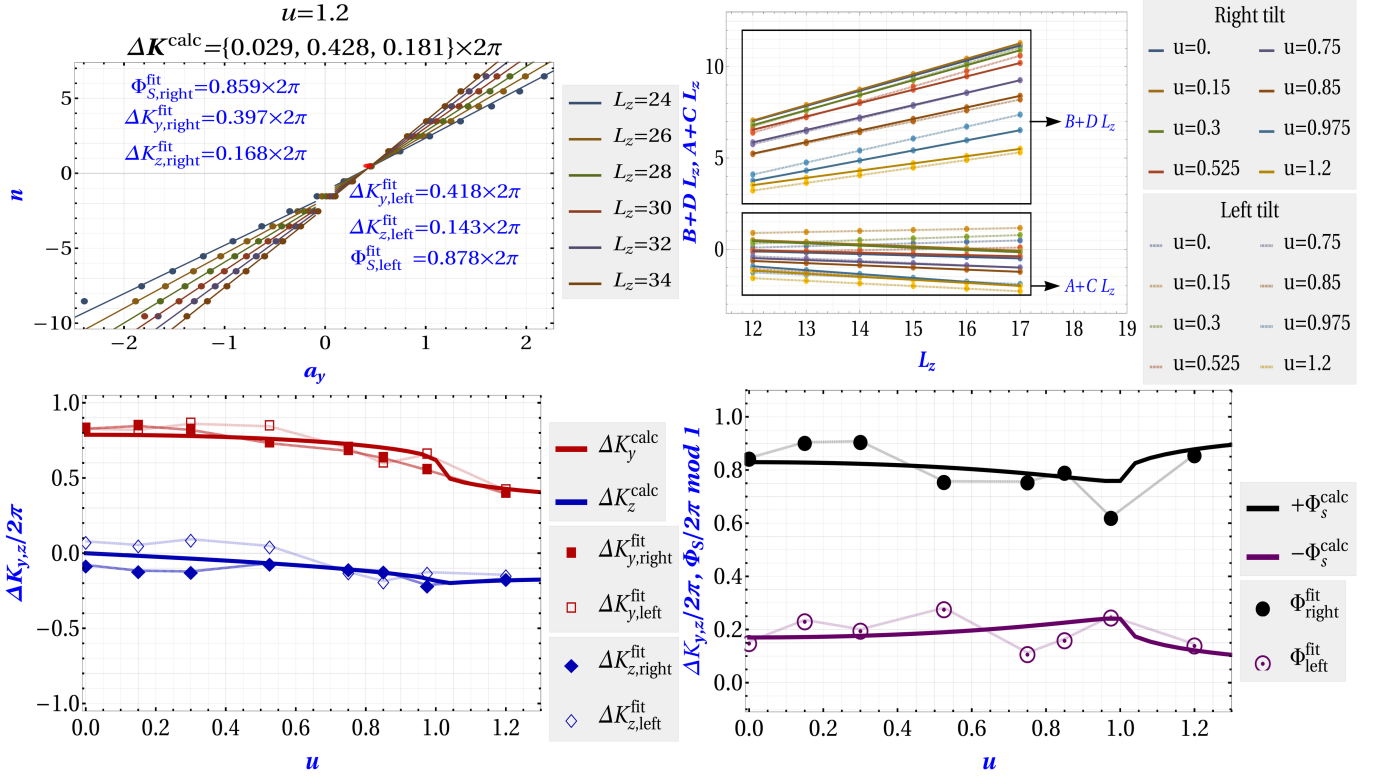


FIG. 4 Detailed numerical fits. Top left: Zero modes indices (j) vs a_y fit well to straight lines for each L_z , but separately for $a_y > 0$ (“right”) and $a_y < 0$ (“left”). Fitting the slopes and intercepts to straight lines in L_z , as shown on the top right, allows extracting Φ_S , ΔK_y and ΔK_z numerically, which match well with their values calculated from the band structure. Bottom left: The calculated and fitted values of $\Delta K_{y,z}$ are similar and in good agreement and for both $a_y > 0$ and $a_y < 0$. Bottom right: The calculated and fitted values of Φ_S are in good agreement, and are equal and opposite $\text{mod } 2\pi$ for $a_y > 0$ and $a_y < 0$.

while we expect

$$\Phi_{\text{tot}}(L_z, a_y) = \Phi_S + \Delta K_y d a_y + \Delta K_z L_z + \Delta K_y a_y L_z \quad (14)$$

It is important that fitting is performed separately for $a_y > 0$ and $a_y < 0$. This is because the semiclassical orbits for the two cases encircle the vortex in opposite directions and acquire equal and opposite Φ_S , but yield the same values for the other parameters. Moreover, zero modes near $a_y = 0$ must be ignored because they involve interference between clockwise and counterclockwise orbits around the vortex, which causes deviations from the semiclassical limit. We also ignore zero modes for large $|a_y|$, corresponding to vortex ends being near the edge of the lattice.

Comparing (13) and (14), we extract the values of ΔK_y , ΔK_z , Φ_S and d . The first three parameters match remarkably well with values calculated directly in the normal state while d gives $\Phi_S + 2\Delta \mathbf{K} \cdot \mathbf{d} \approx \pi$ at the magic angle as expected.

C. Φ_S as a Berry phase on a Bloch sphere

The lattice model defined by Eq. (8) admits an elegant analytical determination of Φ_S , which facilitates comparison with the vortex numerics.

As stated in Sec. V A, FAs occur along curves where $d_z(\mathbf{k})$ has zero eigenvalues. Assuming $\ell > 0$, (k_x, k_y) satisfy $\sqrt{v_x^2 \sin^2 k_x + v_y^2 \sin^2 k_y} = \ell$ along such a curve while the spin part of the wavefunction is an eigenstate of $\sigma_x v_x \sin k_x + \sigma_y v_y \sin k_y$ with eigenvalue $+\ell$. As a result, the surface projection of a FA state at \mathbf{k} satisfies $\langle \psi_{\mathbf{k},\lambda}^{FA} | \sigma_i | \psi_{\mathbf{k},\lambda}^{FA} \rangle = v_i \sin k_i / \ell$, where $\lambda = \pm 1$ denote a FAs on top (bottom) surface, while the spin rotates by

an angle

$$\phi = \arg \left(\frac{v_x \sin K_x^2 + i v_y \sin K_y^2}{v_x \sin K_x^1 + i v_y \sin K_y^1} \right) \quad (15)$$

along a FA that connects surface projections of Weyl nodes at \mathbf{K}^1 and \mathbf{K}^2 . Moreover, $|\psi_{\mathbf{k},\lambda}^{FA}\rangle$ satisfy

$$[\tau_x d_x(\mathbf{k}, -i\partial_z) + \tau_y d_y(\mathbf{k}, -i\partial_z)] |\psi_{\mathbf{k},\lambda}^{FA}\rangle = 0 \quad (16)$$

which immediately implies that $|\psi_{\mathbf{k},\lambda}^{FA}\rangle$ are Jackiw-Rebbi zero modes in bilayer space, spanned by τ_i . In particular, they are eigenstates of τ_z with opposite eigenvalues on the top and bottom surface. To determine Φ_S , we view the σ and τ degrees of freedom as two spin-1/2 particles, and consider the effect of the above rotations on the total spin, $\mathbf{S} = (\boldsymbol{\tau} + \boldsymbol{\sigma})/2$.

Table I describes the four segments of a semiclassical orbit involving Weyl nodes at \mathbf{K}_1 and \mathbf{K}_2 in terms of both $\boldsymbol{\tau} \otimes \boldsymbol{\sigma}$ and \mathbf{S} .

| Segment | Behavior in $\boldsymbol{\tau} \otimes \boldsymbol{\sigma}$ | Behavior in \mathbf{S} |
|----------------------|---|--|
| Top surface FA | Rotation of $\langle \boldsymbol{\sigma} \rangle$ about σ_z by ϕ , with fixed $\langle \boldsymbol{\tau} \rangle = (0, 0, 1)$. | Rotation of $\langle \mathbf{S} \rangle$ about S_z by ϕ with fixed $\langle S_z \rangle = 1/2$. |
| Downward bulk travel | π rotation of $\langle \boldsymbol{\tau} \rangle$ from $(0, 0, 1)$ to $(0, 0, -1)$ with fixed $\langle \boldsymbol{\sigma} \rangle$. | Rotation of $\langle \mathbf{S} \rangle$ from $\langle S_z \rangle = +1/2$ to $\langle S_z \rangle = -1/2$ with fixed $\langle S_x \rangle, \langle S_y \rangle$. |
| Bottom surface FA | Rotation of $\langle \boldsymbol{\sigma} \rangle$ about σ_z by $-\phi$, with fixed $\langle \boldsymbol{\tau} \rangle = (0, 0, -1)$. | Rotation of $\langle \mathbf{S} \rangle$ about S_z by ϕ with fixed $\langle S_z \rangle = -1/2$. |
| Upward bulk travel | π rotation of $\langle \boldsymbol{\tau} \rangle$ from $(0, 0, -1)$ to $(0, 0, 1)$ with fixed $\langle \boldsymbol{\sigma} \rangle$. | Rotation of $\langle \mathbf{S} \rangle$ from $\langle S_z \rangle = -1/2$ to $\langle S_z \rangle = +1/2$ with fixed $\langle S_x \rangle, \langle S_y \rangle$. |

TABLE I Description of the four segments of a semiclassical orbit in bilayer-spin space, $\boldsymbol{\tau} \otimes \boldsymbol{\sigma}$, and in terms of total spin, $\mathbf{S} = (\boldsymbol{\tau} + \boldsymbol{\sigma})/2$. The angle ϕ is given in Eq. (15).

On the Bloch sphere for total spin, these segments define a patch with area $\phi \times [\frac{1}{2} - (-\frac{1}{2})] = \phi$, as shown in Fig. 5. This patch induces a Berry phase $S\phi$, which vanishes in the singlet sector ($S = 0$) and equals ϕ in the triplet sector ($S = 1$). Thus, the total Berry phase acquired through the above rotations is

$$\Phi_S = \phi \quad (17)$$

where ϕ is given in Eq. (15).

We acknowledge financial support from the National Science Foundation grant DMR-2047193.

-
- [1] C Caroli, P. G. De Gennes, and J Matricon. Bound Fermion states on a vortex line in a type II superconductor. *Physics Letters*, 9(4):307–309, may 1964. [I](#)
 - [2] N Read and Dmitry Green. Paired states of fermions in two dimensions with breaking of parity and time-reversal symmetries and the fractional quantum Hall effect. *Phys. Rev. B*, 61(15):10267–10297, apr 2000. [I](#)
 - [3] Liang Fu and C L Kane. Superconducting Proximity Effect and Majorana Fermions at the Surface of a Topological Insulator. *Phys. Rev. Lett.*, 100(9):96407, mar 2008. [I](#), [III](#), [III](#)
 - [4] A.Yu. Kitaev. Fault-tolerant quantum computation by anyons. *Annals of Physics*, 303(1):2–30, 2003. [I](#)
 - [5] Jason Alicea. New directions in the pursuit of majorana fermions in solid state systems. *Reports on Progress in Physics*, 75(7), 2012. [III](#)

-
- [6] C W J Beenakker. Search for Majorana Fermions in Superconductors. *Annual Review of Condensed Matter Physics*, 4(1):113–136, 2013.
 - [7] Steven R. Elliott and Marcel Franz. Colloquium: Majorana fermions in nuclear, particle, and solid-state physics. *Reviews of Modern Physics*, 87(1), 2015. [III](#)
 - [8] Leo Kouwenhoven. Majorana Qubits. *Technical Digest - International Electron Devices Meeting, IEDM*, 2018-Decem:6.6.1—6.6.4, 2019.
 - [9] R M Lutchyn, E P A M Bakkers, L P Kouwenhoven, P Krogstrup, C M Marcus, and Y Oreg. Majorana zero modes in superconductor–semiconductor heterostructures. *Nature Reviews Materials*, 3(5):52–68, 2018.
 - [10] Ning Ma. Majorana fermions in condensed matter: An outlook. *Physica B: Condensed Matter*, 512(January):100–101, 2017. [I](#), [III](#)
 - [11] Peng Zhang, Peng Zhang, Koichiro Yaji, Takahiro Hashimoto, Yuichi Ota, Takeshi Kondo, Kozo Okazaki, Zhijun Wang, Jinsheng Wen, G D Gu, Hong Ding, Shik Shin, Peng Zhang, Koichiro Yaji, Takahiro Hashimoto, Yuichi Ota, Takeshi Kondo, Kozo Okazaki, Zhijun Wang, Jinsheng Wen, G D Gu, Hong Ding, and Shik Shin. Observation of topological superconductivity on the surface of an iron-based superconductor. *Science*, 360(April):182, 2018. [I](#), [III](#)
 - [12] Lingyuan Kong, Shiyu Zhu, Hui Papaj Michaland Chen, Lu Cao, Hiroki Isobe, Yuqing Xing, Wen Yao Liu, Dongfei Wang, Peng Fan, Yujie Sun, Shixuan Du, John Schneeloch, Ruidan Zhong, Genda Gu, Liang Fu, Hong-Jun Gao, and Hong Ding. Half-integer level shift of vortex bound states in an iron-based superconductor. *Nature Physics*, 15(11):1181–1187, 2019. [III](#)

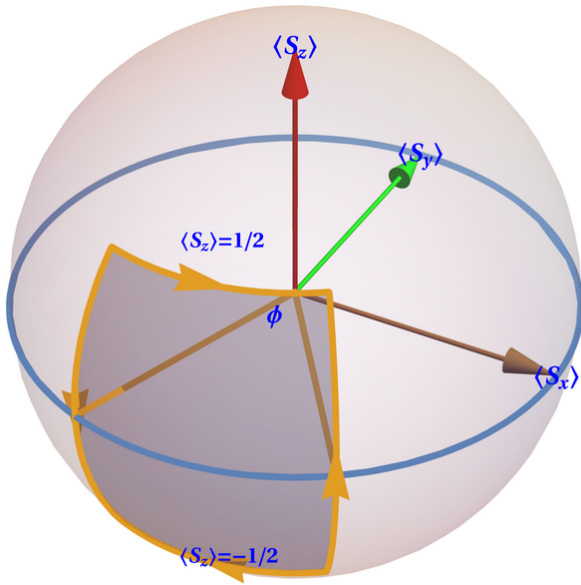


FIG. 5 Semi-classical orbit (yellow curve) on the $S = 1$ Bloch sphere that results from the triplet combination of the spin (σ) and bilayer pseudo-spin (τ) degrees of freedom. Horizontal (vertical) arms of the orbit capture motion along the FAs (through the bulk) and yield a Berry phase equal to the solid angle enclosed by the orbit.

- [13] Shiyu Zhu, Lingyuan Kong, Lu Cao, Hui Chen, Michał Papaj, Shixuan Du, Yuqing Xing, Wenyao Liu, Dongfei Wang, Chengmin Shen, Fazhi Yang, John Schneeloch, Ruidan Zhong, Genda Gu, Liang Fu, Yu-Yang Zhang, Hong Ding, and Hong-Jun Gao. Nearly quantized conductance plateau of vortex zero mode in an iron-based superconductor. *Science*, 367(6474):189–192, 2020.
- [14] Dongfei Wang, Lingyuan Kong, Peng Fan, Hui Chen, Shiyu Zhu, Wenyao Liu, Lu Cao, Yujie Sun, Shixuan Du, John Schneeloch, Ruidan Zhong, Genda Gu, Liang Fu, Hong Ding, and Hong-Jun Gao. Evidence for Majorana bound states in an iron-based superconductor. *Science*, 362(6412):333–335, 2018.
- [15] T. Machida, Y. Sun, S. Pyon, S. Takeda, Y. Kohsaka, T. Hanaguri, T. Sasagawa, and T. Tamegai. Zero-energy vortex bound state in the superconducting topological surface state of Fe(Se,Te). *Nature Materials*, 18(8):811–815, 2019. [III](#)
- [16] Qin Liu, Chen Chen, Tong Zhang, Rui Peng, Ya Jun Yan, Chen Hao Ping Wen, Xia Lou, Yu Long Huang, Jin Peng Tian, Xiao Li Dong, Guang Wei Wang, Wei Cheng Bao, Qiang Hua Wang, Zhi Ping Yin, Zhong Xian Zhao, and Dong Lai Feng. Robust and Clean Majorana Zero Mode in the Vortex Core of High-Temperature Superconductor (Li_{0.84}Fe_{0.16})OHFeSe. *Physical Review X*, 8(4):41056, dec 2018. [III](#)
- [17] Wenyao Liu, Lu Cao, Shiyu Zhu, Lingyuan Kong, Guangwei Wang, Michał Papaj, Peng Zhang, Ya-Bin Liu, Hui Chen, Geng Li, Fazhi Yang, Takeshi Kondo, Shixuan Du, Guang-Han Cao, Shik Shin, Liang Fu, Zhiping Yin, Hong-Jun Gao, and Hong Ding. A new majorana platform in an fe-as bilayer superconductor. *Nature Communications*, 11(1):5688, 2020.
- [18] Lingyuan Kong, Lu Cao, Shiyu Zhu, Michał Papaj, Guangyang Dai, Geng Li, Peng Fan, Wenyao Liu, Fazhi Yang, Xiancheng Wang, Shixuan Du, Changqing Jin, Liang Fu, Hong-Jun Gao, and Hong Ding. Majorana zero modes in impurity-assisted vortex of lifeas superconductor. *Nature Communications*, 12(1):4146, 2021.
- [19] Zhijun Wang, P. Zhang, Gang Xu, L. K. Zeng, H. Miao, Xiaoyan Xu, T. Qian, Hongming Weng, P. Richard, A. V. Fedorov, H. Ding, Xi Dai, and Zhong Fang. Topological nature of the fese_{0.5}te_{0.5} superconductor. *Phys. Rev. B*, 92:115119, Sep 2015. [III](#)
- [20] X.-L. Peng, Y. Li, X.-X. Wu, H.-B. Deng, X. Shi, W.-H. Fan, M. Li, Y.-B. Huang, T. Qian, P. Richard, J.-P. Hu, S.-H. Pan, H.-Q. Mao, Y.-J. Sun, and H. Ding. Observation of topological transition in high- T_c superconducting monolayer fete_{1-x}se_x films on srtio₃(001). *Phys. Rev. B*, 100:155134, Oct 2019.
- [21] Gang Xu, Biao Lian, Peizhe Tang, Xiao-Liang Qi, and Shou-Cheng Zhang. Topological Superconductivity on the Surface of Fe-Based Superconductors. *Phys. Rev. Lett.*, 117(4):47001, jul 2016. [III](#)
- [22] Peng Zhang, Zhijun Wang, Xianxin Wu, Koichiro Yaji, Yukiaki Ishida, Yoshimitsu Kohama, Guangyang Dai, Yue Sun, Cedric Bareille, Kenta Kuroda, Takeshi Kondo, Kozo Okazaki, Koichi Kindo, Xiancheng Wang, Changqing Jin, Jiangping Hu, Ronny Thomale, Kazuki Sumida, Shilong Wu, Koji Miyamoto, Taichi Okuda, Hong Ding, G D Gu, Tsuyoshi Tamegai, Takuto Kawakami, Masatoshi Sato, and Shik Shin. Multiple topological states in iron-based superconductors. *Nature Physics*, 15(1):41–47, 2019.
- [23] Shengshan Qin, Lunhui Hu, Xianxin Wu, Xia Dai, Chen Fang, Fu-Chun Zhang, and Jiangping Hu. Topological vortex phase transitions in iron-based superconductors. *Science Bulletin*, 64(17):1207–1214, 2019.
- [24] Areg Ghazaryan, Pedro L. S. S Lopes, Pavan Hosur, Matthew J Gilbert, and Pouyan Ghaemi. Effect of Zeeman coupling on the Majorana vortex modes in iron-based topological superconductors. *Phys. Rev. B*, 101(2):20504, jan 2020. [I](#)
- [25] N P Armitage, E J Mele, and Ashvin Vishwanath. Weyl and Dirac semimetals in three-dimensional solids. *Rev. Mod. Phys.*, 90(1):15001, jan 2018. [I](#)
- [26] Ari M. A. M. Turner and Ashvin Vishwanath. Beyond Band Insulators: Topology of Semi-metals and Interacting Phases. *ArXiv e-prints*, jan 2013.
- [27] A A Burkov. Weyl Metals. *Annual Review of Condensed Matter Physics*, 9(1):359–378, 2018.
- [28] Shun-Qing Shen. Topological Dirac and Weyl Semimetals. In *Topological Dirac and Weyl Semimetals*. Springer series in solid-state sciences, 2017.
- [29] Sumathi Rao. Weyl semi-metals: A short review. *Journal of the Indian Institute of Science*, 96(2), 2016.
- [30] Binghai Yan and Claudia Felser. Topological Materials: Weyl Semimetals. *Annual Review of Condensed Matter Physics*, 8(1):337–354, 2017.
- [31] P. Hosur, A. Kapitulnik, S.A. Kivelson, J. Orenstein, and S. Raghu. Kerr effect as evidence of gyrotropic order in the cuprates. *Physical Review B - Condensed Matter and*

- Materials Physics*, 87(11), 2013.
- [32] Huichao Wang and Jian Wang. Electron transport in Dirac and Weyl semimetals. *Chinese Physics B*, 27(10):107402, oct 2018. [I](#)
- [33] P. Hosur, P. Ghaemi, R.S.K. Mong, and A. Vishwanath. Majorana modes at the ends of superconductor vortices in doped topological insulators. *Physical Review Letters*, 107(9), 2011. [II](#), [III](#), [III](#), [III](#)
- [34] Ashvin Vishwanath. *Vortices, quasiparticles and unconventional superconductivity*. PhD thesis, Princeton University, jan 2001. [II](#)
- [35] Rauf Giwa and Pavan Hosur. Fermi arc criterion for surface Majorana modes in superconducting time-reversal symmetric Weyl semimetals. *Physical Review Letters*, 127(18):187002, jun 2021. [II](#), [III](#), [III](#)
- [36] Jan Borchmann and T Pereg-Barnea. Quantum oscillations in Weyl semimetals: A surface theory approach. *Phys. Rev. B*, 96(12):125153, sep 2017. [II](#)
- [37] Andrew C Potter, Itamar Kimchi, and Ashvin Vishwanath. Quantum oscillations from surface Fermi arcs in Weyl and Dirac semimetals. *Nature Communications*, 5(1):1–6, oct 2014.
- [38] Y. Zhang, D. Bulmash, P. Hosur, A.C. Potter, and A. Vishwanath. Quantum oscillations from generic surface Fermi arcs and bulk chiral modes in Weyl semimetals. *Scientific Reports*, 6, 2016. [II](#)
- [39] Tudor D Stanescu, Jay D Sau, Roman M Lutchyn, and S Das Sarma. Proximity effect at the superconductor-topological insulator interface. *Physical Review B - Condensed Matter and Materials Physics*, 2010. [III](#)
- [40] Roman M Lutchyn, Tudor D Stanescu, and S Das Sarma. Search for Majorana fermions in multiband semiconducting nanowires. *Physical Review Letters*, 106(12):1–4, 2011. [III](#)
- [41] V. Mourik, K. Zuo, S. M. Frolov, S. R. Plissard, E. P.A.M. Bakkers, and L. P. Kouwenhoven. Signatures of majorana fermions in hybrid superconductor-semiconductor nanowire devices. *Science*, 336(6084):1003–1007, 2012. [III](#)
- [42] Gang Xu, Biao Lian, Peizhe Tang, Xiao-Liang Qi, and Shou-Cheng Zhang. Topological superconductivity on the surface of fe-based superconductors. *Physical Review Letters*, 117:047001, Jul 2016. [III](#)
- [43] Andreas Aste. A direct road to majorana fields. *Symmetry*, 2(4):1776–1809, 2010. [III](#)
- [44] Liang Fu and C. L. Kane. Superconducting proximity effect and majorana fermions at the surface of a topological insulator. *Physical Review Letters*, 100(9):96407, 2008.
- [45] A Yu Kitaev. Unpaired majorana fermions in quantum wires. *Physics-Uspekhi*, 44(10S):131–136, oct 2001.
- [46] Martin Leijnse and Karsten Flensberg. Introduction to topological superconductivity and Majorana fermions. *Semiconductor Science and Technology*, 27(12), 2012.
- [47] Xiao Ping Liu, Yuan Zhou, Yi Fei Wang, and Chang De Gong. Characterizations of topological superconductors: Chern numbers, edge states and majorana zero modes. *New Journal of Physics*, 19(9), 2017.
- [48] N Mohanta and A Taraphder. Topological superconductivity and Majorana bound states at the LaAlO₃/SrTiO₃ interface. *Epl*, 108(6), 2014.
- [49] Stevan Nadj-Perge, Ilya K Drozdov, Jian Li, Hua Chen, Sangjun Jeon, Jungpil Seo, Allan H MacDonald, B Andrei Bernevig, and Ali Yazdani. Observation of Majorana fermions in ferromagnetic atomic chains on a superconductor. *Science*, 346(6209):602–607, 2014.
- [50] Xiao Liang Qi and Shou Cheng Zhang. Topological insulators and superconductors. *Reviews of Modern Physics*, 83(4), 2011.
- [51] N. Read and Dmitry Green. Paired states of fermions in two dimensions with breaking of parity and time-reversal symmetries and the fractional quantum hall effect. *Physical Review B - Condensed Matter and Materials Physics*, 2000.
- [52] Leonid P. Rokhinson, Xinyu Liu, and Jacek K. Furdyna. The fractional a.c. josephson effect in a semiconductor-superconductor nanowire as a signature of majorana particles. *Nature Physics*, 8(11):795–799, 2012.
- [53] Masatoshi Sato and Satoshi Fujimoto. Existence of Majorana fermions and topological order in nodal superconductors with spin-orbit interactions in external magnetic fields. *Physical Review Letters*, 105(21):1–4, 2010.
- [54] Masatoshi Sato and Yoichi Ando. Topological superconductors: A review. *Reports on Progress in Physics*, 80(7):1–45, 2017. [III](#)
- [55] Elio J König, Piers Coleman, Elio J König, and Piers Coleman. Crystalline-Symmetry-Protected Helical Majorana Modes in the Iron Pnictides. *Physical Review Letters*, 122(20), 2019. [III](#)
- [56] Zhongbo Yan, Zhigang Wu, and Wen Huang. Vortex end majorana zero modes in superconducting dirac and weyl semimetals. *Phys. Rev. Lett.*, 124:257001, Jun 2020.
- [57] Shengshan Qin, Lunhui Hu, Xianxin Wu, Xia Dai, Chen Fang, Fu-Chun Zhang, and Jiangping Hu. Topological vortex phase transitions in iron-based superconductors. *Science Bulletin*, 64(17):1207–1214, 2019. [III](#)
- [58] Y. Ran, P. Hosur, and A. Vishwanath. Fermionic Hopf solitons and Berry phase in topological surface superconductors. *Physical Review B - Condensed Matter and Materials Physics*, 84(18), 2011. [III](#)
- [59] Ching Kai Chiu, Jeffrey C Y Teo, Andreas P Schnyder, and Shinsei Ryu. Classification of topological quantum matter with symmetries. *Reviews of Modern Physics*, 88(3):1–70, 2016. [III](#)
- [60] Pavan Hosur. Friedel oscillations due to Fermi arcs in Weyl semimetals. *Physical Review B - Condensed Matter and Materials Physics*, 86(19):1–5, 2012. [V A](#)